



OPEN *Operando* detection of dissolved oxygen in fluid solution using a submersible rapid scan EPR on a chip dipstick sensor

Joseph E. McPeak^{1,2}✉, Michele Segantini¹, Gianluca Marcozzi¹, Irene Dona¹, Silvio Künstner¹, Anh Chu³, Michal Kern³, Martin Poncelet^{4,5}, Benoit Driesschaert^{4,5}, Jens Anders^{3,6} & Klaus Lips^{1,7}

Electron paramagnetic resonance (EPR) is an accurate and efficient technique to probe unpaired electrons in many applications across materials science, chemistry, and biology. Dynamic processes are investigated using EPR; however, these applications are limited by the use of resonator-based spectrometers such that the entire process must be confined to the resonator. The EPR-on-a-chip (EPRoC) device circumvents this limitation by integrating the entire EPR spectrometer into a single microchip. In this approach, the coil of a voltage-controlled oscillator (VCO) is used as the microwave source and detector simultaneously, operating under a protective coating such that the device may be placed in the sample solution directly. Additionally, improvements in sensitivity via rapid scan EPR (RS-EPR/RS-EPRoC) increase the accessible applications where SNR per measurement time is the fundamental limit. The herein reported device combines a dipstick EPRoC sensor with the enhanced sensitivity of frequency-swept frequency modulated rapid scan to measure triarylmethyl (trityl, Ox071) oxygen-sensitive probes dissolved in aqueous solutions. EPR spectra of Ox071 solutions were recorded using the RS-EPRoC sensor while varying the oxygen concentration of the solution between normal atmosphere and after purging the solution with nitrogen gas. We demonstrate that EPRoC may be employed to monitor dissolved oxygen in fluid solution in an online fashion.

Keywords Operando, Dipstick, Rapid scan EPR, Oximetry, EPR-on-a-chip (EPRoC), Sensor

Electron paramagnetic resonance (EPR) is a spectroscopic technique to probe the environment of unpaired electrons spins that has found use in many applications ranging from materials science, chemistry, biology, healthcare, and even medical imaging¹. Though it is primarily employed as a tool in fundamental research, there has been growing interest over the last several decades in the adaptation of EPR methods to medical diagnostics. Assessment of local oxygen concentration is paramount in a plethora of peripheral diagnostics such as wound healing, blood oxygen content, tissue oxygenation, and in identifying cardiovascular diseases as well as for assessment of brain function^{2–4}. Oxygen consumption, which is often investigated simultaneously with oxygen concentration, is also implicated in oxidative stress and plays a particularly important role in mitochondrial function^{5–7}. These processes are underpinned by the production of reactive oxygen species (ROS) which cause significant cellular damage and therefore are of particular importance for the overall assessment of human health^{2,5–7}. For this reason several probe molecules have been developed to interrogate these processes using EPR spectroscopy, such as solid probes like lithium phthalocyanine and soluble probes such as nitroxides and triarylmethyl (trityl) radicals^{8–14}. Of these, the trityl probes have shown the most promise in clinical applications due to their increased stability in biological media^{14–17}.

¹Berlin Joint EPR Laboratory and EPR4Energy, Department Spins in Energy Conversion and Quantum Information Science (ASPIN), Helmholtz-Zentrum Berlin für Materialien und Energie GmbH, Berlin, Germany. ²Department of Chemistry, Novo Nordisk Foundation Pulse EPR Center, University of Copenhagen, Copenhagen, Denmark. ³Institute of Smart Sensors, Universität Stuttgart, Stuttgart, Germany. ⁴Department of Pharmaceutical Sciences, School of Pharmacy, West Virginia University, Morgantown, WV, USA. ⁵In Vivo Multifunctional Magnetic Resonance Center, Robert C. Byrd Health Sciences Center, West Virginia University, Morgantown, WV, USA. ⁶Center for Integrated Quantum Science and Technology (IQST), Stuttgart and Ulm, Germany. ⁷Berlin Joint EPR Laboratory, Fachbereich Physik, Freie Universität Berlin, Berlin, Germany. ✉email: Joseph.mcpeak@helmholtz-berlin.de

One of the most advantageous reporting schemes employing EPR methods is the assessment of local oxygen concentration in the context of EPR imaging, similar to how nuclear magnetic resonance (NMR) spectroscopy has experienced widespread adoption via magnetic resonance imaging (MRI) methods routinely used in the clinic and has even been used to map oxygen concentration in tumors in both preclinical and clinical trials^{16–20}. Ex-vivo methods of measuring oxygen concentration have been employed to show effects of oxygen in cell-death, antioxidant transcription, cell proliferation, and acute inflammation; and, more recently EPR imaging has been incorporated into well plates for high throughput measurements of biological samples^{21,22}. While toxicity towards cells and other biological samples is a major concern, another drawback to the utilization of EPR methods in medical assessment is the requirement for a paramagnetic spin probe or reporter molecule that is sufficiently tailored to the information desired from the living organism.^{1417,1916,182–45–72,5–78–1414–17}

EPR spectroscopy is well suited for the task of reporting the local concentration of oxygen via paramagnetic triarylmethyl probes (Fig. 1). While molecular oxygen possesses radical characteristics, relaxation occurs too rapidly to detect it. However, the molecular collision interaction of the carbon-centered triarylmethyl (trityl) radical probes with molecular oxygen may be accurately assessed via lineshape broadening in the trityl EPR spectra^{3,15,23}. The inherently narrow lines of trityl radicals provide excellent oxygen sensitivity^{24–26}. Through careful calibration, the linewidth of the trityl accurately reports on the local oxygen concentration while EPR imaging methods provide a spatial distribution of the trityl EPR signal, forming a diagnostic map of the local environment that is useful for treatment^{3,15}.

While the narrow linewidth of trityl probes improves resolution for oximetry, narrow linewidths are typically indicative of slow relaxation and can lead to saturation effects using conventional EPR methods²⁷. Trityl radical relaxation times are on the order of microseconds, a regime where pulse EPR methods have proven more advantageous; however, rapid scan (RS) EPR has been shown to produce the greatest increase in signal-to-noise ratios (SNR) relative to conventional continuous wave (CW) methods^{28,29}. This improvement is primarily observed due to reduction of saturation effects, accomplished by adiabatic passage through resonance while subsequent deconvolution of the rapid passage effects allows undistorted narrow linewidths of these spin systems to be obtained^{30–32}. Because SNR is highly dependent on resonator quality factor (Q), rapid scan experiments have typically been performed in high Q resonators while rapidly sweeping the microwave field using small sweep coils that offset the main magnetic field during the EPR experiment^{30–32}. The rapid sweep rates used in rapid scan require broadband detection to accurately deconvolve rapid passage effects, which inversely affects resonator Q and may reduce SNR or introduce distortions in lineshape³³. Because the aqueous environment typically utilized for trityl measurements creates an ideal environment for broadband measurements due to dielectric effects leading to microwave absorption, rapid scan is an effective method for trityl EPR oximetry measurements³⁴. In other cases the resonator Q must be lowered significantly to obtain undistorted spectra, often through complicated techniques which are not compatible with *operando* experiments^{35,36}.

EPR-on-a-chip (EPRoC) devices have recently been demonstrated to perform EPR spectroscopy without the use of an EPR resonator by performing both excitation and detection of the spin signal response using voltage-

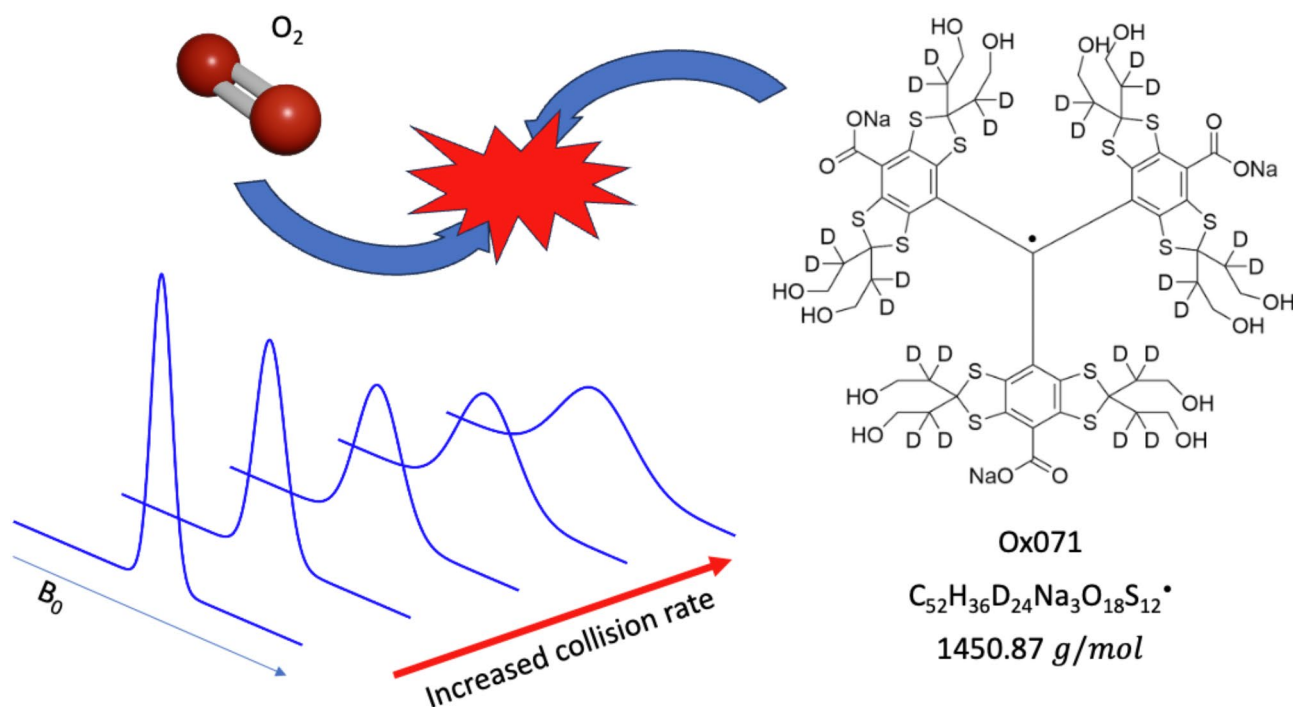


Fig. 1. An overview of oxygen monitoring via EPR where the monitoring capabilities of the probe molecule are dependent on the collisional interactions with radical-oxygen species, detectable as a linewidth-dependent change in the relaxation rate of the trityl spin probe, Ox071.

controlled oscillators (VCOs)^{37–41}. In this application, the cavity resonator is replaced by a single coil inductor and varactor, which function primarily in a similar fashion as the inductive-capacitive (LC) circuitry of a typical resonator (Fig. 2a). However, this lumped LC resonator may be interfaced to a cross coupled transistor pair providing a negative resistance capable of replenishing the energy lost in the LC resonator. While the primary purpose of this is to offset the conductive loss in the coil, losses due to high dielectric constant materials that absorb microwaves, which are significantly smaller than the overall coil loss, are also replenished^{40,42–44}. By embedding the VCO in a phase-locked loop (PLL) circuit, its phase and frequency may be controlled both precisely and with very short response time by varying the reference frequency to create a wide (up to GHz) frequency sweep range for EPR spectroscopy⁴⁵. The pseudo-high Q broadband circuit is facilitated by changing the oscillation frequency of the coil directly via manipulation of the varactor inside the VCO, which is controlled through the PLL by the reference frequency provided by a radio-frequency generator (Fig. 2b)⁴⁶. The EPRoC is therefore ideal for detection of trityl radicals in the aqueous environment used for oximetry measurements. When properly isolated from the solvent via a protective coating (parlylene C), the EPRoC may be used as a dipstick sensor for detection of free radicals directly in solution⁴⁷.

Though the EPRoC has previously been demonstrated to perform frequency-swept rapid scan EPR with significantly improved SNR relative to CW EPR, slowly relaxing spin centers still pose a challenge for the EPRoC due to the inherently high microwave excitation (B_1), primarily due to the required bias current to produce stable oscillations in the small (200 μm) VCO^{48–50}. Therefore, CW spectra recorded using the high intensity B_1 of the EPRoC may exhibit saturation induced line broadening and lineshape distortions⁵⁰. For this reason, a detection scheme similar to dispersion EPR has been developed via frequency-swept, frequency modulated rapid scan (Fig. 2c)^{51–54}. In this way, the typical saturation of the absorption lineshape, obtained via amplitude modulation of the VCO, is circumvented both by recording the dispersion-like lineshape via frequency modulation, and by utilizing the increased B_1 possible due to rapid passage through resonance with rapid scan^{48,55,56}. Coupled with the fast digitization possible with rapid scan, it is feasible to accurately record the trityl lineshape with respect to dissolved oxygen concentration in fluid solution on a timescale relevant for real-time monitoring⁴⁸.

Combining these methodologies in a single operational device, we herein present *operando* and in situ assessment of oxygen concentration using the well-characterized trityl radical probe, Ox071, in fluid solution using a frequency-swept, frequency modulated rapid scan EPRoC dipstick device. By submerging the EPRoC directly in the reaction solution, EPR spectra are obtained that provide adequate lineshape resolution and sufficient SNR to correlate the observed linewidths with the time-dependent concentration of dissolved oxygen directly in solution without additional modification to the sample environment.

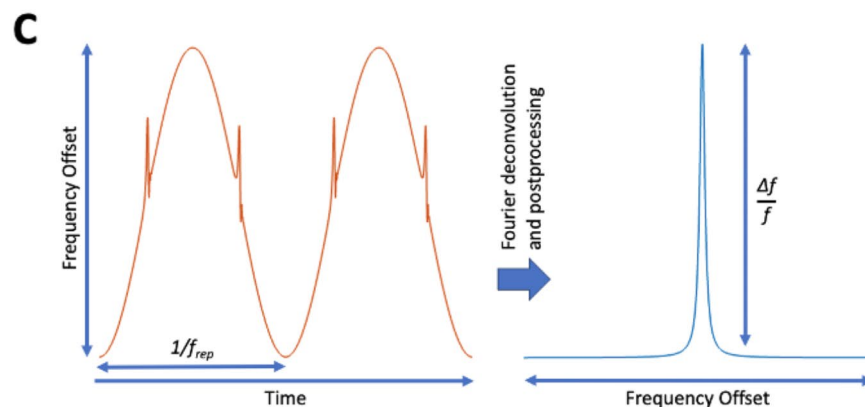
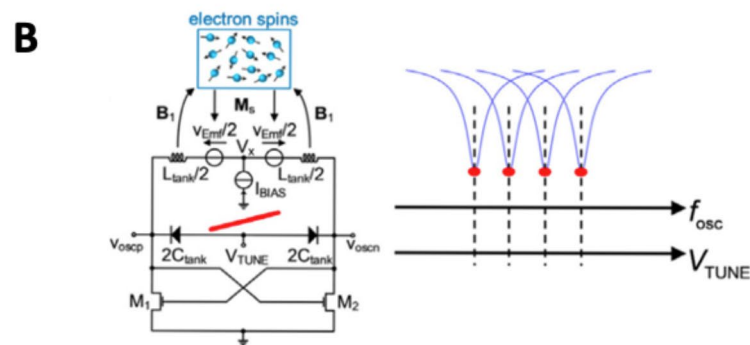
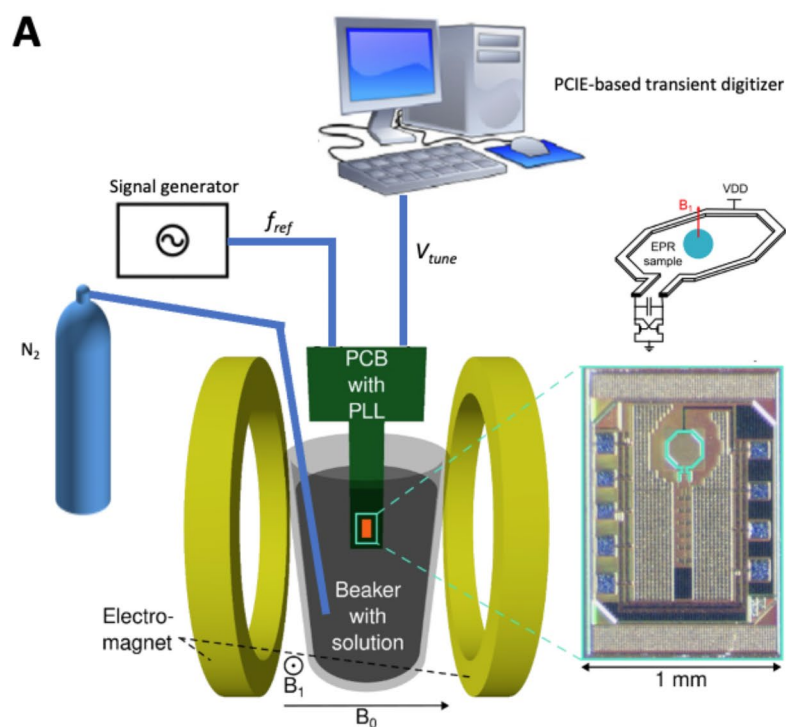
Materials and methods

Sample solutions

The trityl probe molecule, Ox071, was synthesized as reported previously^{57,58}. Upon successful synthesis, the spin probe was dissolved in a dilute phosphate-buffered saline solution containing 150 mM sodium chloride, 3 mM potassium chloride, 10 mM disodium hydrogen phosphate dihydrate, and 2 mM potassium phosphate (PBS Buffer pH 7.6 -10x conc., Jena Bioscience) to a final concentration of approximately 0.3 mM, which is comparable to previously reported clinical applications^{17,22}.

Instrument configuration

For RS-EPRoC experiments, the trityl solution was placed in a 20 ml beaker positioned in the center of a Bruker B-E 25 electromagnet. The EPRoC printed circuit board (PCB) was attached to a supporting rod which provided an interface to a stepper motor (Thorlabs PT3-Z8) that allows the lowering and lifting of the EPRoC PCB into and out of the solution. The design principles of EPRoC devices have been presented extensively elsewhere but are briefly described here for convenience^{37–40,42–48,50,59}. The EPRoC chip contains a VCO oscillating at a frequency of around 13.44 GHz and a divide-by-32 frequency divider, the output of which is fed into an on-chip buffer used to embed the VCO in a phase-locked loop located on the PCB. To provide the reference frequency (f_{ref}) for the PLL of the EPRoC, a signal generator (Rohde & Schwarz SMB100B) operating at 420 MHz was used. The sinusoidal modulation was applied directly to the reference frequency such that a frequency deviation (f_{dev}) of 83.2 MHz was obtained at a repetition rate (f_{rep}) of 35 kHz resulting in a scan rate of 18.3 THz/s, equivalent to 6.5 MG/s field sweeps. The required signal bandwidth for unattenuated detection considering the narrow linewidth of the Ox071 was between 18 and 60 MHz while the bandwidth of the EPRoC PLL for rapid scan detection was 5 MHz (see *Supp.* Fig S1). The 5 MHz bandwidth is limited by the parasitic capacitance and inductance present on the PCB traces. There have been other EPRoC designs which integrate the entire PLL circuit on-chip and have hence achieved much larger bandwidths up to 200 MHz^{49,60,61}. Because of a voltage offset present in the EPRoC FM signal, a 20 dB AC coupled amplifier (Mini-Circuits Model ZFL-500LN) with a 20 dB attenuator placed on the input for a total zero gain amplification which allowed the signal intensity to be within the dynamic range of the transient digitizer (ADQ7DC, Teledyne SP Devices). The rapid scan signal was recorded using a sampling rate of 5 GS/s. A bias current (4 mA) defining the magnitude of B_1 was supplied to the EPRoC PCB by a low noise current source (Keithley 6221). Dry nitrogen was flowed through the trityl solution by way of a flexible tube submerged directly into the trityl solution. Evacuation of oxygen was continued for \approx 6 hours using relatively slow flow rates as to not alter the volume of the solution. Before beginning measurements, the flow of nitrogen was removed to further reduce the likelihood of concentration fluctuations during EPR measurements. The reoxygenation of the trityl solution was then monitored continuously by recording a RS-EPRoC spectrum at 30 s intervals. The acquisition time for each spectrum was 19 s and consisted of 70,000 accumulations, each containing seven frequency-swept spectra which were then summed during post-processing.



Analysis of Operando measurements

Rapid scan measurements were performed by submersing the EPRoC in the Ox071 solution, followed by removal of oxygen via dry nitrogen gas to establish the minimum obtainable linewidth. Spectral acquisition parameters were optimized to reduce total acquisition time while maintaining sufficient SNR for accurate linewidth measurements. After six hours of purging with dry nitrogen gas, the Ox071 solution EPR spectrum was recorded sequentially during the reoxygenation process by acquiring a rapid scan spectrum every 30 s. Each spectrum was then baseline corrected to remove the sinusoidal background typical of rapid scan experiments using a composite sinusoidal fit and subsequent least-squares analysis before subtraction from the directly digitized frequency-swept spectra. The baseline corrected spectra were then separated by direction of the sweep, either via increasing frequency or decreasing frequency, and summed before being separately Fourier deconvolved to derive the resulting EPR signal^{48,63}. The dispersion-like lineshapes were then Hilbert transformed using the

◀ **Fig. 2.** (a) An overview of the instrument configuration used for the experiments concerning oxygen detection using the EPRoC dipstick. An external oscillator provides the RF reference signal for the PLL. The single coil (diameter 200 μ m) EPRoC was coated with a 10–12 μ m thick layer of parylene C and submerged into the solution. The RS data were recorded using the digitizer (b) Operating principle of the EPRoC showing the bi-directional coupling of the VCO to the electron spins. Changing the reference oscillator frequency results in a change of the VCO oscillation frequency via the varactor inside the VCO while the cross-coupled transistor pair provides a negative resistance. This acts to mitigate loss in the coil and loss while maintaining a pseudo-high Q circuit at every oscillation frequency. (c) The detection scheme utilized for frequency-swept, frequency-modulated rapid scan detection. The periodic signal is recorded in the time domain by sinusoidally sweeping the VCO with an amplitude f_{dev} and repetition rate f_{rep} . The resulting periodic spin signal is Fourier deconvolved to recover the slow scan signal, detected as a spin-induced change in oscillator frequency, $\Delta f/f$, as the VCO is swept through resonance. Adapted from Refs^{40,47,62}.

Kramers-Kronig relation to obtain absorption-like lineshapes in order to be comparable with CW experiments performed using a conventional spectrometer (see *Supp.*) and with prior results reported in the literature using Ox071⁶⁴.

The evolution of the linewidth over time during the reoxygenation process was monitored by fitting each absorption spectrum with a Lorentzian function,

$$y = \frac{2}{\pi \sqrt{3}} \times \frac{1}{\Gamma} \times \frac{1}{1 + \frac{4}{3} \left(\frac{x - B_0}{\Gamma} \right)^2} \quad (1)$$

where Γ is the distance between the inflection points and B_0 is the resonance value which have been estimated by least-square minimization using the *esfit* function included in the software package EasySpin 6 (<https://easyspin.org>)⁶⁵. The values of Γ have been plotted with respect to time to determine the rate at which the linewidth of the trityl signal was broadened by increasing oxygen concentration. This was achieved by fitting via an exponential function,

$$\Gamma(t) = -A \exp(-\alpha \cdot t) + c \quad (2)$$

where $\Gamma(t)$ is the linewidth obtained at time t , α is the rate constant of the reoxygenation process, t is the time, A is the amplitude of the exponential change and c is the equilibrium value after the complete reoxygenation to atmospheric conditions. The time constant of the reoxygenation was calculated from the fit using the following relation, $\tau = \alpha^{-1}$.

Estimation of the partial pressure of oxygen

To estimate the partial pressure of oxygen, the relationship between the partial pressure of oxygen in solution and the linewidth of Ox071 (2 mM) recorded via free induction decay (FID) detected 2D-phantom EPR imaging at 300 MHz from Ref¹⁵ was modified to yield the following relationship,

$$pO_2 = \frac{\Gamma(t) - q - n}{\sqrt{3} m} \quad (3)$$

where q is the linear offset obtained, n is a concentration broadening parameter often referred to as self-broadening and m is the angular coefficient reported in Ref¹⁵. Due to differences between the methods used to record the EPR spectrum reported in Ref¹⁵, where FID detection was used, and the methods reported herein, where instead the Hilbert transformed data were used. Therefore to compare the minimum linewidth observed in the herein reported experiments (50 mG) and those reported in Ref¹⁵ (90 mG), the partial pressure of oxygen differs by a factor of the square root of three and is necessary due to the inclusion of this factor in Eq. 1 to be comparable with data recorded by CW (see *Supp.*).

Results

Frequency-swept, frequency-modulated rapid scan EPR measurements were performed using the EPRoC dipstick device on the trityl-containing solutions in presence of oxygen and after ≈ 6 hours of purging the solutions with dry-nitrogen gas. The spectra obtained, from which the linewidths were determined by *Lorentzian* fitting, are shown in Fig. 3. For the Ox071 solution, the oxygenated linewidth observed was 160 mG and the deoxygenated linewidth was 50 mG.

To determine the potential to monitor reoxygenation of the trityl solution with respect to time, multiple frequency-swept, frequency-modulated rapid scan transients were continuously recorded after evacuation of oxygen using a continuous flow of dry nitrogen gas bubbled through the solution. Once a minimum linewidth in the deconvolved spectra was obtained, the nitrogen flow was stopped and the rapid scan signal was recorded. The reoxygenation was treated as an exponential process, and the fit to the linewidths obtained with respect to time for each sample is shown in Fig. 4.

Using the deoxygenated linewidth in the rapid scan experiments as a calibration factor, the approximate partial pressure of oxygen was obtained for the data shown in Fig. 4 using the relationship described in Eq. 3. A linear relationship may be obtained utilizing all linewidths recorded between the minimum and maximum linewidths observed. After inclusion of all consideration necessary for comparison due to discrepancies between

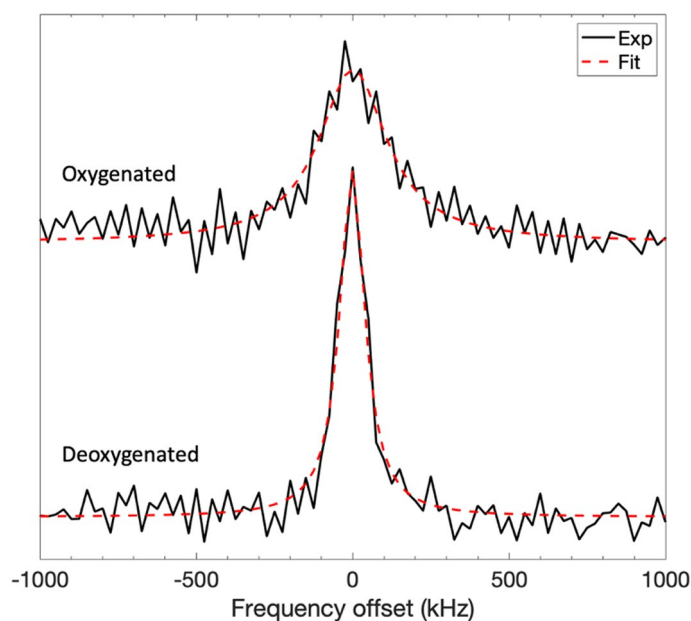


Fig. 3. EPR spectra obtained via Hilbert transformation of the frequency-swept, frequency modulated rapid scan spectra obtained with the EPRoC for the trityl radical investigated, Ox071, shown both before and after evacuation of oxygen by purging with nitrogen gas. Fits to the data obtained by Lorentzian fitting are overlaid on the appropriate spectrum.

data collection methods, the change in partial pressure of oxygen with respect to linewidth using the EPRoC sensor was found to be 0.53 mmHg O₂ per kHz, equivalent to 1.47 mmHg O₂ per mG. The detectable range observed using the EPRoC device is therefore approximately between zero and 140 mmHg O₂.

Discussion

In comparison to linewidths obtained via CW for trityl probes reported (see *Supp.* Fig S2), the linewidths observed in RS-EPRoC experiments demonstrate that the EPRoC sensor was successfully employed to detect dissolved oxygen over the range obtainable by nitrogen evacuation in aqueous environments which are typically problematic for EPR measurements at these frequencies (X-band) due to microwave absorption of the solvent⁶⁶. Here, the VCO circuit is largely immune to dielectric loss from aqueous solvents, creating a stable B₁ field throughout all measurements due to the negative resistance provided by the active pump circuit via the cross-coupled transistor pair and the comparatively lower E₁ fields present relative to a typical cavity resonator^{40,42–44}. It was observed in the experiments performed that the degree of saturation of the trityl systems was low enough to permit Kramers-Kronig transformations to an absorption-like lineshape (see *Supp.*); however, correction of the detected signal by phase manipulation was not possible due to the lack of quadrature detection⁶⁷. Even with a presumed admixture of absorption and dispersion and the saturation observed, a calibration may be performed using solutions with known partial pressures of oxygen to accurately allow the EPRoC to function as an oxygen sensor.

Based on prior experiments, the expected linewidth change is approximately 1.45 mmHg O₂ per mG while the EPRoC device reports 0.53 mmHg O₂ per kHz, equivalent to 1.47 mmHg O₂ per mG using Ox071 which is in considerably good agreement¹⁵. The experiments were performed with the solution open to the environment without additional modifications. The deoxygenated values are in agreement with prior reports, on the order of 50 mG; however, additional broadening was observed as the reoxygenation of the solution was recorded. It has been demonstrated in prior work that the VCO generates a substantial amount of heat during operation due to the power consumption of the device in a relatively small area (~30 mW/mm²) and this is the likely cause for the broadening at higher oxygen concentrations⁶⁸. Because the N₂ flow is removed before beginning to record the slow reoxygenation of such a large sample volume, there is no longer any method for removing the heat generated by the coils and therefore this significant heat generation likely causes the temperature of the water near the VCO to rise significantly. The heat produced cannot be easily removed or dissipated without an additional cooling mechanism. Because this is a reproducible phenomenon, the accuracy of the device in an oxygen-sensing environment is likely unaffected; however, the sensitivity suffers and is evidenced by the increased variability in the later measurements.

While field swept rapid scan imposes significant challenges associated with the increasing of scan rate due to the high voltages (≈ kV) required for rapid field sweeps, the frequency-swept, FM detection scheme circumvents these limitations because only the microwave frequency is swept^{69,70}. This not only allows access to much wider sweep widths, but also allows for much faster scan rates as reported in ref⁴⁸. One major drawback to frequency-swept, FM-detected rapid scan is the integration of noise over the entire frequency sweep (83.2 MHz). While the resonator acts as a bandwidth limitation in resonator-based rapid scan, it also acts as an effective noise filter

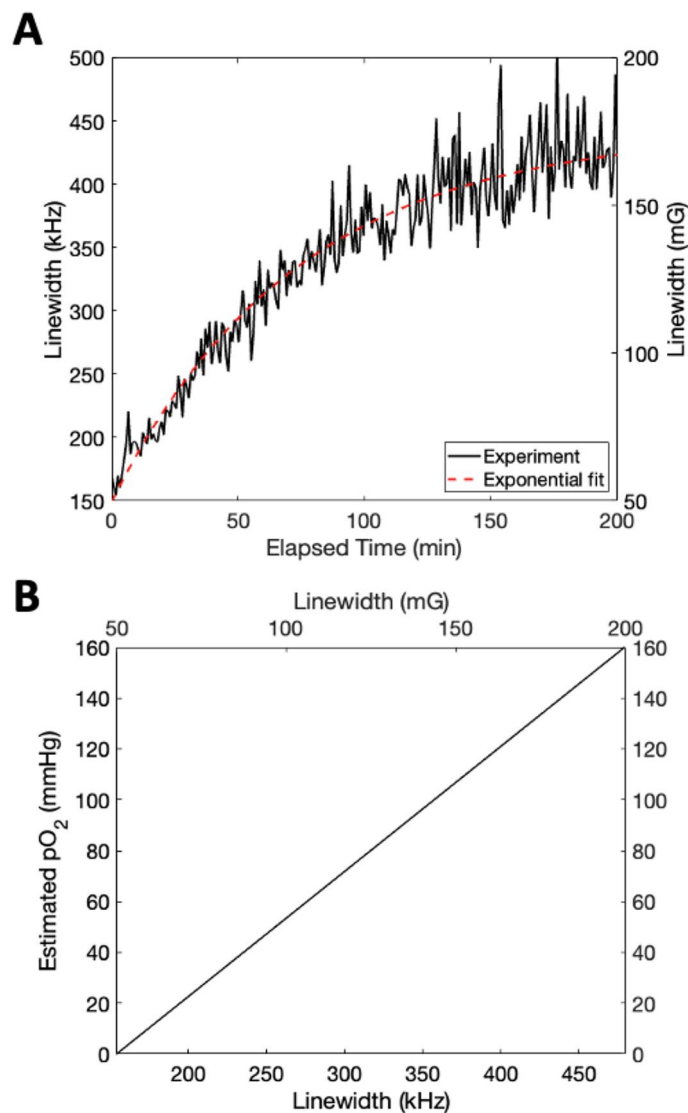


Fig. 4. (a) The linewidth of the resulting EPR spectrum for each trityl as a function of reoxygenation time after stopping the flow of nitrogen through the solution via frequency-swept, frequency modulated rapid scan using the EPRoC sensor. The standard deviation of the measurements after reaching equilibrium was approximately 30 kHz. (b) The linewidth vs. oxygen (partial pressure) obtained via frequency-swept, frequency modulated rapid scan EPR using the dipstick EPRoC sensor via Eq. 3 using $q = 7.637$ mG, $m = 0.1257$ mG/mmHg, and $n = 0.1726$ mG.

that rejects all frequencies outside the bandwidth of the resonator (see *Supp. Fig S3*)⁷¹. Field-swept rapid scan inherently generates less noise in the acquired spectrum because of this; however, given the high resolution with which transient data may be recorded, digital filters with wide window functions can be applied to the recorded spectra in post-processing to improve the SNR. The standard deviation of the reoxygenated spectra after reaching equilibrium (~30 kHz) is primarily the result of a large inherent noise present when using VCOs and may be improved by increasing the number of VCOs in the array. This concept is further described in the supplementary information provided. The standard deviation reported here was calculated after reaching equilibrium, where the SNR for trityl measurements is lowest; therefore, this is the maximum observable standard deviation and is thereby reduced when lower oxygen concentrations are present, improving reproducibility. This may be further improved using higher trityl concentrations which may then be tailored to the range of oxygen concentration values of interest after consideration of concentration-dependent broadening effects.

When considering prior rapid scan experiments using EPRoC devices, it is possible to perform frequency-swept, AM-detected rapid scan with significant SNR improvements over CW-EPR within the same timescale; however, in the current design of the EPRoC devices, AM-detection is limited to a single coil⁴⁸. Injection-locking has been recently demonstrated as a viable method to increase the sensitivity of EPRoC devices in a way that multiple coils may be used to produce a global phase-coherent microwave excitation field⁴³. This reduces the

complexity of a multicoil device by allowing the spin-induced frequency shift of the VCOs to be detected as a single FM output signal^{40,48}.

One of the unique benefits of frequency-swept, frequency modulated rapid scan experiments is the alleviation of excitation bandwidth constraints imposed by the resonator in resonator-based rapid scan experiments. Because the frequency is swept at a rate that is rapid relative to spin diffusion, the entire sweep range of the VCO may be utilized for spin-excitation without distorting the spin response. In this way the detection system becomes the limiting bandwidth while the spin system is homogeneously excited, even if the PLL bandwidth limits the SNR of the detection due to filtering, but not distortion, of the high-frequency components of the rapid scan signal⁴⁸. This bandwidth limit imposes a cutoff frequency beyond which the signal intensity is attenuated; however, the spin response is not altered and the lineshape is free of distortions induced by incomplete or nonuniform excitation due to limited resonator-bandwidth.

In both resonator-based EPR and in frequency-swept, FM-detected rapid scan, the fundamental spin sensitivity is defined by the sample with respect to number of spins comprising the total linewidth. In resonator-based CW-EPR the sensitivity is also defined by the Q factor of the resonator, the filling factor of the resonator, and the signal averaging rate which is determined by the digitizer and the ramp rate of the electromagnet⁷². In frequency-swept, FM-detected rapid scan the sensitivity does not suffer from low Q observed with solvent systems; and, given the design of the dipstick sensor, the filling factor is improved by way of submerging the detector in an apparent large volume relative to the detector coil diameter. Though less than half of the effective volume is utilized in the current design, EPRoCs compatible with microfluidics measurements improve upon this concept and may be incorporated into future fully-submersible applications^{47,61,73}. While the sensitivity suffers in the herein reported rapid scan experiments due to the low repetition rate of the frequency sweep, this can be alleviated by utilizing higher bandwidth (on-chip) PLL circuits, like those that have successfully been demonstrated in pulse-EPRoC applications^{49,61}.

Conclusions and outlook

In this report we have demonstrated the *operando* and in situ capabilities of a submersible EPR-on-a-chip device capable of monitoring the concentration of dissolved oxygen using the trityl spin probe, Ox071. By using frequency-swept frequency-modulated rapid scan EPR methods, the limits on excitation bandwidth have been effectively circumvented resulting in EPR spectra that may be recorded on a timescale relevant for concentration monitoring in real-time. Similarly, the scalability of EPRoC and VCO based rapid scan techniques has been expanded by incorporation of the frequency-modulated EPRoC signal, which may be recorded in multiple coils of a VCO array, thereby removing both the volume limitations imposed by the small volume of a single coil and the scaling limitations imposed by amplitude-modulated rapid scan detection in EPRoC devices. The methods reported herein while applied to the application for oximetry may be generally applied to any spin system of interest that falls within the bandwidth of the EPRoC device; and, when narrow linewidths are not necessary, may also be applied in applications where a lower-homogeneity permanent magnet might be used. Because of the scalability of EPRoC devices, new geometries, increased coil diameters (to several mm), and even distributions of EPRoC VCO arrays may be considered, such as incorporation into a needle or other surgical devices to establish a spatial component while also considering mesh arrays or even more complicated geometries for surface-accessible diagnostics^{22,74}. All of these advancements will allow the EPRoC to continue to progress and evolve as a point-of-care technology.

Data availability

The datasets used and/or analyzed during the current study are available from the corresponding author on reasonable request.

Received: 25 September 2024; Accepted: 7 March 2025

Published online: 21 March 2025

References

1. Brustolon, M. & Giamello, E. (eds) *Electron Paramagnetic Resonance: A Practitioner's Toolkit* (Wiley, 2009). <https://doi.org/10.1002/9780470432235>.
2. Liu, S., Timmins, G. S., Shi, H., Gasparovic, C. M. & Liu, K. J. Application of *in vivo* EPR in brain research: monitoring tissue oxygenation, blood flow, and oxidative stress. *NMR Biomed.* **17** (5), 327–334. <https://doi.org/10.1002/nbm.899> (2004).
3. Ahmad, R., Kuppasamy, P. & Theory Instrumentation, and applications of electron paramagnetic resonance oximetry. *Chem. Rev.* **110** (5), 3212–3236. <https://doi.org/10.1021/cr900396q> (2010).
4. Swartz, H. M. et al. Clinical EPR: unique opportunities and some challenges. *Acad. Radiol.* **21** (2), 197–206. <https://doi.org/10.1016/j.acra.2013.10.011> (2014).
5. Halliwell, B. & Gutteridge, J. M. C. *Free Radicals in Biology and Medicine* (Oxford University Press, 2015). <https://doi.org/10.1093/acprof:oso/9780198717478.001.0001>.
6. Donatienne, H. et al. A versatile EPR toolbox for the simultaneous measurement of oxygen consumption and superoxide production. *Redox Biol.* **40**, 101852. <https://doi.org/10.1016/j.redox.2020.101852> (2021).
7. Mariappan, N., Elks, C. M., Fink, B., Francis, J. & TNF-Induced Mitochondrial Damage: A link between mitochondrial complex I activity and left ventricular dysfunction. *Free Radic Biol. Med.* **46** (4), 462–470. <https://doi.org/10.1016/j.freeradbiomed.2008.10.049> (2009).
8. Martin, R. M. et al. Toward a nanoencapsulated EPR imaging agent for clinical use. *Mol. Imaging Biol.* <https://doi.org/10.1007/s11307-023-01863-0> (2023).
9. Gallez, B. et al. Small particles of fusinite and carbohydrate Chars coated with aqueous soluble polymers: Preparation and applications for *in vivo* EPR oximetry. *Magn. Reson. Med.* **40** (1), 152–159. <https://doi.org/10.1002/mrm.1910400120> (1998).
10. Ilangovan, G., Li, H., Zweier, J. L. & Kuppasamy, P. Electrochemical Preparation and EPR Studies of Lithium Phthalocyanine. 3. Measurements of Oxygen Concentration in Tissues and Biochemical Reactions. <https://doi.org/10.1021/jp010130+> (2001).

11. Zweier, J. L., Chzhan, M., Ewert, U., Schneider, G. & Kuppusamy, P. Development of a highly sensitive probe for measuring oxygen in biological tissues. *J. Magn. Reson. B.* **105** (1), 52–57. <https://doi.org/10.1006/jmrb.1994.1099> (1994).
12. Bobko, A. A. et al. Trityl-Based EPR probe with enhanced sensitivity to oxygen. *Free Radic Biol. Med.* **47** (5), 654–658. <https://doi.org/10.1016/j.freeradbiomed.2009.06.007> (2009).
13. Khramtsov, V. V. In Vivo spectroscopy and imaging of nitroxide probes. In *Nitroxides - Theory, Experiment and Applications; InTech*, <https://doi.org/10.5772/39129>. (2012).
14. Dunn, J. F. & Swartz, H. M. In vivo electron paramagnetic resonance oximetry with particulate materials. *Methods* **30** (2), 159–166. [https://doi.org/10.1016/S1046-2023\(03\)00077-X](https://doi.org/10.1016/S1046-2023(03)00077-X) (2003).
15. Matsumoto, K. et al. EPR-based oximetric imaging: A combination of single Point-based Spatial encoding and T1 weighting. *Magn. Reson. Med.* **80** (5), 2275–2287. <https://doi.org/10.1002/mrm.27182> (2018).
16. Gertsenshteyn, I. et al. Absolute Oxygen-Guided Radiation Therapy Improves Tumor Control in Three Preclinical Tumor Models. *Front Med (Lausanne)* **10**. <https://doi.org/10.3389/fmed.2023.1269689> (2023).
17. Epel, B., Viswakarma, N., Sundramoorthy, S. V., Pawar, N. J. & Kotecha, M. Oxygen imaging of a rabbit tumor using a Human-Sized pulse electron paramagnetic resonance imager. *Mol. Imaging Biol.* <https://doi.org/10.1007/s11307-023-01852-3> (2023).
18. Walsh, J. C. et al. The clinical importance of assessing tumor hypoxia: relationship of tumor hypoxia to prognosis and therapeutic opportunities. *Antioxid. Redox Signal.* **21** (10), 1516–1554. <https://doi.org/10.1089/ars.2013.5378> (2014).
19. Schaner, P. E. et al. OxyChip Implantation and Subsequent Electron Paramagnetic Resonance Oximetry in Human Tumors Is Safe and Feasible: First Experience in 24 Patients. *Front. Oncol.* **10**. <https://doi.org/10.3389/fonc.2020.572060> (2020).
20. Epel, B., Redler, G. & Halpern, H. J. *Oxygen Transport to Tissue XXXVI*; Swartz, H. M., Harrison, D. K., Bruley, D. F., Eds.; Advances in Experimental Medicine and Biology; Springer New York: New York, NY, Vol. 812. <https://doi.org/10.1007/978-1-4939-0620-8> (2014).
21. Ruigrok, M. J. R. et al. The effects of oxygen concentration on cell death, Anti-Oxidant transcription, acute inflammation, and cell proliferation in Precision-Cut lung slices. *Sci. Rep.* **9** (1), 16239. <https://doi.org/10.1038/s41598-019-52813-2> (2019).
22. Hameed, S. et al. Longitudinal, 3D oxygen imaging of cells in a Multi-Well plate using pulse electron paramagnetic resonance imaging. *Npj Imaging.* **2** (1), 8. <https://doi.org/10.1038/s44303-024-00013-7> (2024).
23. Ardenkjær-Larsen, J. H. et al. EPR and DNP properties of certain novel single electron contrast agents intended for oximetric imaging. *J. Magn. Reson.* **133** (1), 1–12. <https://doi.org/10.1006/jmre.1998.1438> (1998).
24. Yong, L. et al. Electron spin relaxation of triarylmethyl radicals in fluid solution. *J. Magn. Reson.* **152** (1), 156–161. <https://doi.org/10.1006/jmre.2001.2379> (2001).
25. Subramanian, S. et al. Noninvasive in vivo oximetric imaging by radiofrequency FT EPR. *Magn. Reson. Med.* **47** (5), 1001–1008. <https://doi.org/10.1002/mrm.10133> (2002).
26. Williams, B. B. et al. Imaging spin probe distribution in the tumor of a living mouse with 250 mhz EPR: correlation with BOLD MRI. *Magn. Reson. Med.* **47** (4), 634–638. <https://doi.org/10.1002/mrm.10089> (2002).
27. Eaton, S. S. & Eaton, G. R. Relaxation mechanisms. *eMagRes* **5** (4), 1543–1556. <https://doi.org/10.1002/9780470034590.emrstm1507> (2016).
28. Owenius, R., Eaton, G. R. & Eaton, S. S. Frequency (250 MHz to 9.2 GHz) and viscosity dependence of electron spin relaxation of triarylmethyl radicals at room temperature. *J. Magn. Reson.* **172** (1), 168–175. <https://doi.org/10.1016/j.jmr.2004.10.007> (2005).
29. Mitchell, D. G. et al. X-Band Rapid-Scan EPR of samples with long electron spin relaxation times: A comparison of continuous wave, pulse and Rapid-Scan EPR. *Mol. Phys.* **111** (18–19), 2664–2673. <https://doi.org/10.1080/00268976.2013.792959> (2013).
30. Eaton, S. S. et al. Rapid-Scan EPR imaging. *J. Magn. Reson.* **280**, 140–148. <https://doi.org/10.1016/j.jmr.2017.02.013> (2017).
31. Joshi, J. P. et al. Rapid-Scan EPR with triangular scans and fourier Deconvolution to recover the Slow-Scan spectrum. *J. Magn. Reson.* **175** (1), 44–51. <https://doi.org/10.1016/j.jmr.2005.03.013> (2005).
32. Tseitlin, M., Rinard, G. A., Quine, R. W., Eaton, S. S. & Eaton, G. R. Deconvolution of sinusoidal rapid EPR scans. *J. Magn. Reson.* **208** (2), 279–283. <https://doi.org/10.1016/j.jmr.2010.11.015> (2011).
33. Eaton, G. R., Eaton, S. S. & Rapid-Scan Electron. *Paramagnetic Reson.* *eMagRes* **5** (4), 1529–1542. <https://doi.org/10.1002/9780470034590.emrstm1522>. (2016).
34. Nesmelov, Y. E., Gopinath, A. & Thomas, D. D. Aqueous sample in an EPR cavity: sensitivity considerations. *J. Magn. Reson.* **167** (1), 138–146. <https://doi.org/10.1016/j.jmr.2003.12.005> (2004).
35. Mitchell, D. G., Quine, R. W., Tseitlin, M., Eaton, S. S. & Eaton, G. R. X-Band Rapid-Scan EPR of nitroxyl radicals. *J. Magn. Reson.* **214**, 221–226. <https://doi.org/10.1016/j.jmr.2011.11.007> (2012).
36. Eaton, G. R. & Eaton, S. S. Advances in rapid scan EPR spectroscopy. In *Methods in Enzymology*; Academic Press Inc. Vol. 666, 1–24. <https://doi.org/10.1016/bs.mie.2022.02.013> (2022).
37. Handwerker, J. et al. 28.2 A 14GHz Battery-Operated Point-of-Care ESR Spectrometer Based on a 0.13µm CMOS ASIC. In *IEEE International Solid-State Circuits Conference (ISSCC)*; IEEE, 2016; pp 476–477. <https://doi.org/10.1109/ISSCC.2016.7418114> (2016).
38. Yalcin, T. & Boero, G. Single-Chip detector for electron spin resonance spectroscopy. *Rev. Sci. Instrum.* **79** (9). <https://doi.org/10.1063/1.2969657> (2008).
39. Schlecker, B. et al. VCO-Based ESR-on-a-Chip as a tool for Low-Cost, High-Sensitivity Point-of-Care diagnostics. In 2017 IEEE SENSORS; IEEE, 1–3. <https://doi.org/10.1109/ICSENS.2017.8233896>. (2017).
40. Anders, J. & Lips, K. MR to go. *J. Magn. Reson.* **306**, 118–123. <https://doi.org/10.1016/j.jmr.2019.07.007> (2019).
41. Yang, X., Babakhani, A. A. & Single-Chip Electron paramagnetic resonance transceiver in 0.13-Mm SiGe BiCMOS. *IEEE Trans. Microw. Theory Tech.* **63** (11), 3727–3735. <https://doi.org/10.1109/TMTT.2015.2481895> (2015).
42. Razavi, B. The Cross-Coupled Pair - Part I [A circuit for all seasons]. *IEEE Solid-State Circuits Mag.* **6** (3), 7–10. <https://doi.org/10.1109/MSSC.2014.2329234> (2014).
43. Chu, A., Schlecker, B., Lips, K., Ortman, M. & Anders, J. An 8-Channel 13GHz ESR-on-a-Chip Injection-Locked Vco-Array Achieving 200µM-Concentration Sensitivity. In *IEEE International Solid - State Circuits Conference - (ISSCC)*; IEEE, 2018; pp 354–356. <https://doi.org/10.1109/ISSCC.2018.8310330> (2018).
44. Chu, A. et al. On the modeling of Amplitude-Sensitive electron spin resonance (ESR) detection using Voltage-Controlled oscillator (VCO)-Based ESR-on-a-Chip detectors. *Magn. Reson.* **2** (2), 699–713. <https://doi.org/10.5194/mr-2-699-2021> (2021).
45. Anders, J. Nonlinear modeling of Continuous-Wave spin detection using Oscillator-Based ESR-on-a-Chip sensors. In *Studies in systems, decision and control. Springer Int. Publishing.* **109**, 57–87. https://doi.org/10.1007/978-3-319-58996-1_4 (2018).
46. Chu, A. et al. VCO-Based ESR-on-a-Chip as a Tool for Low-Cost, High-Sensitivity Food Quality Control. In 2017 IEEE Biomedical Circuits and Systems Conference (BioCAS); IEEE, ; pp 1–4 (2017). <https://doi.org/10.1109/BIOCAS.2017.8325172>.
47. Künstner, S. et al. Monitoring the state of charge of vanadium redox flow batteries with an EPR-on-a-Chip dipstick sensor. *Phys. Chem. Chem. Phys.* **26** (25), 17785–17795. <https://doi.org/10.1039/D4CP00373J> (2024).
48. Künstner, S. et al. Rapid-Scan electron paramagnetic resonance using an EPR-on-a-Chip sensor. *Magn. Reson.* **2** (2), 673–687. <https://doi.org/10.5194/mr-2-673-2021> (2021).
49. Hassan, M. A. et al. A 14-Channel 7 GHz VCO-Based EPR-on-a-Chip Sensor with Rapid Scan Capabilities. In 2021 IEEE Sensors; Vol. 2021-October, pp 1–4. <https://doi.org/10.1109/SENSOR47087.2021.9639513> (2021).
50. Künstner, S. et al. Microwave Field Mapping for EPR on a Chip Experiments. *Sci Adv Accepted.* (2024).
51. Laguta, O., Tuček, M., van Slageren, J. & Neugebauer, P. Multi-Frequency Rapid-Scan HFEP. *J. Magn. Reson.* **296**, 138–142. <https://doi.org/10.1016/j.jmr.2018.09.005> (2018).

52. Hyde, J. S., Strangeway, R. A., Camenisch, T. G., Ratke, J. J. & Froncisz, W. W. -Band Frequency-Swept EPR. *J. Magn. Reson.* **205** (1), 93–101. <https://doi.org/10.1016/j.jmr.2010.04.005> (2010).
53. Hyde, J. S. et al. Microwave frequency modulation in CW EPR at W-Band using a Loop-Gap resonator. *J. Magn. Reson.* **185** (2), 259–263. <https://doi.org/10.1016/j.jmr.2007.01.002> (2007).
54. Segantini, M. et al. Compact Electron Paramagnetic Resonance on a Chip Spectrometer Using a Single Sided Permanent Magnet. *ACS Sens Submitted.* (2024).
55. Hyde, J. S., Froncisz, W. & Kusumi, A. Dispersion electron spin resonance with the Loop-Gap resonator. *Rev. Sci. Instrum.* **53** (12), 1934–1937. <https://doi.org/10.1063/1.1136918> (1982).
56. Rinard, G. A., Quine, R. W., Ghim, B. T., Eaton, S. S. & Eaton, G. R. Dispersion and superheterodyne EPR using a bimodal resonator. *J. Magn. Reson. A.* **122** (1), 58–63. <https://doi.org/10.1006/jmra.1996.0174> (1996).
57. Poncet, M., Huffman, J. L., Khramtsov, V. V., Dhimitruka, I. & Driesschaert, B. Synthesis of hydroxyethyl Tetrathiatriarylmethyl radicals OX063 and OX071. *RSC Adv.* **9** (60), 35073–35076. <https://doi.org/10.1039/C9RA08633A> (2019).
58. Poncet, M. et al. Synthesis and characterization of a biocompatible 13C1 isotopologue of trityl radical OX071 for in vivo EPR viscometry. *Analyst* **147** (24), 5643–5648. <https://doi.org/10.1039/D2AN01527G> (2022).
59. Anders, J., Fully-Integrated, C. M. O. S. & Lausanne Probes for Magnetic Resonance Applications, EPFL. <https://doi.org/10.5075/epfl-thesis-5154> (2011).
60. Khan, K. et al. A 12.2 to 14.9 GHz Injection-Locked VCO Array with an on-Chip 50 MHz BW Semi-Digital PLL for Transient Spin Manipulation and Detection. In *2022 IEEE 65th International Midwest Symposium on Circuits and Systems (MWSCAS)*; IEEE, ; Vol. 2022-August, pp 1–4. (2022). <https://doi.org/10.1109/MWSCAS54063.2022.9859288>.
61. Hassan, M. A. et al. Towards Single-Cell pulsed EPR using VCO-Based EPR-on-a-Chip detectors. *Frequenz* **76**(11–12), 699–717. <https://doi.org/10.1515/freq-2022-0096> (2022).
62. Anders, J. et al. Progress in miniaturization and Low-Field nuclear magnetic resonance. *J. Magn. Reson.* **322**, 106860. <https://doi.org/10.1016/j.jmr.2020.106860> (2021).
63. Stoner, J. W. et al. Direct-Detected Rapid-Scan EPR at 250 MHz. *J. Magn. Reson.* **170** (1), 127–135. <https://doi.org/10.1016/j.jmr.2004.06.008> (2004).
64. Portis, A. M. Electronic structure of F centers: saturation of the electron spin resonance. *Phys. Rev.* **91** (5), 1071–1078. <https://doi.org/10.1103/PhysRev.91.1071> (1953).
65. Stoll, S. & Schweiger, A. EasySpin, a comprehensive software package for spectral simulation and analysis in EPR. *J. Magn. Reson.* **178** (1), 42–55. <https://doi.org/10.1016/j.jmr.2005.08.013> (2006).
66. Dalal, D. P., Eaton, S. S. & Eaton, G. R. The Effects of Lossy Solvents on Quantitative EPR Studies. *J. Magn. Reson.* **44**(3), 415–428. [https://doi.org/10.1016/0022-2364\(81\)90276-6](https://doi.org/10.1016/0022-2364(81)90276-6) (1969).
67. Tseitlin, M., Quine, R. W., Rinard, G. A., Eaton, S. S. & Eaton, G. R. Combining absorption and dispersion signals to improve Signal-to-Noise for Rapid-Scan EPR imaging. *J. Magn. Reson.* **203** (2), 305–310. <https://doi.org/10.1016/j.jmr.2010.01.013> (2010).
68. Segantini, M. et al. Electrically detected magnetic resonance on a chip (EDMRoC) for analysis of Thin-Film silicon photovoltaics. *Magnetochemistry* **9** (7), 183. <https://doi.org/10.3390/magnetochemistry9070183> (2023).
69. Quine, R. W., Mitchell, D. G., Tseitlin, M., Eaton, S. S. & Eaton, G. R. A resonated coil driver for rapid scan EPR. *Concepts Magn. Reson. Part. B Magn. Reson. Eng.* **41B** (4), 95–110. <https://doi.org/10.1002/cmrb.21222> (2012).
70. Quine, R. W., Czechowski, T. & Eaton, G. R. A linear magnetic field scan driver. *Concepts Magn. Reson. Part. B Magn. Reson. Eng.* **35B** (1), 44–58. <https://doi.org/10.1002/cmrb.20128> (2009).
71. Lin, Y. J., Tseng, Y. C. & Wu, T. L. A Resonator-Based suppressor for mitigating the noise transfer on metal plates for control of electromagnetics interference. *IEEE Microwave Wirel. Compon. Lett.* **26** (11), 906–908. <https://doi.org/10.1109/LMWC.2016.2615002> (2016).
72. Eaton, G. R., Eaton, S. S., Barr, D. P., Weber, R. T. & Quantitative, E. P. R. Springer Vienna: Vienna, (2010). <https://doi.org/10.1007/978-3-211-92948-3>
73. Dayan, N. et al. Electron spin resonance microfluidics with subnanoliter liquid samples. *J. Magn. Reson. Open.* **2-3**, 100005. <https://doi.org/10.1016/j.jmro.2020.100005> (2020).
74. Handwerker, J. et al. A CMOS NMR needle for probing brain physiology with high Spatial and Temporal resolution. *Nat. Methods.* **17** (1), 64–67. <https://doi.org/10.1038/s41592-019-0640-3> (2020).

Acknowledgements

We are grateful to Mark Tseytlin for providing the deconvolution algorithm as well as assistance with implementation. We acknowledge Lukas Woodcock for providing the deconvolution script used in these experiments. We also acknowledge Oleksii Laguta for assistance in installation of the PCIe-based digitizer and for providing the necessary scripts for operation and data collection. Development of the dipstick EPRoC was performed with contributions from Peter Fischer and are also acknowledged. We additionally thank the Copenhagen Pulse EPR Facility, supported by a Research Infrastructure - Large Equipment and Facilities grant (NNF21OC0068806) from the Novo Nordisk Foundation.

Author contributions

JM and MS defined the goals of the research. JM, MS, GM, and ID performed the EPR experiments and the data analysis. JM, MS, and SK evaluated the results of the experiments. AC, MK and JA designed the EPRoC device. MP and BD synthesized the trityl spin probes. JM and MS wrote the original manuscript with significant contributions from SK. The manuscript was revised by all authors.

Funding

Open Access funding enabled and organized by Projekt DEAL.

This work has been supported by the Bundesministerium für Bildung und Forschung under contract number 01186916/1 (EPRoC), by the HEMF (Helmholtz Energy Materials Foundry) infrastructure funded by the Helmholtz association (HGF), and by the DFG priority program INTeGrated TERAhertz sYStems Enabling Novel Functionality (INTEREST) (SPP 2314). This work was partially supported by NIH grant (USA): R01EB032321. The content is solely the responsibility of the authors and does not necessarily represent the official views of the NIH.

Declarations

Competing interests

The authors declare no competing interests.

Additional information

Supplementary Information The online version contains supplementary material available at <https://doi.org/10.1038/s41598-025-93591-4>.

Correspondence and requests for materials should be addressed to J.E.M.

Reprints and permissions information is available at www.nature.com/reprints.

Publisher's note Springer Nature remains neutral with regard to jurisdictional claims in published maps and institutional affiliations.

Open Access This article is licensed under a Creative Commons Attribution 4.0 International License, which permits use, sharing, adaptation, distribution and reproduction in any medium or format, as long as you give appropriate credit to the original author(s) and the source, provide a link to the Creative Commons licence, and indicate if changes were made. The images or other third party material in this article are included in the article's Creative Commons licence, unless indicated otherwise in a credit line to the material. If material is not included in the article's Creative Commons licence and your intended use is not permitted by statutory regulation or exceeds the permitted use, you will need to obtain permission directly from the copyright holder. To view a copy of this licence, visit <http://creativecommons.org/licenses/by/4.0/>.

© The Author(s) 2025